Theor Chem Acc (2007) 118:143–148
DOI 10.1007/s00214-007-0257-y

REGULAR ARTICLE

UV-vis spectra of *p*-benzoquinone anion radical in solution by a TD-DFT/PCM approach

Vincenzo Barone · Roberto Improta · Giovanni Morelli · Fabrizio Santoro

Received: 30 October 2006 / Accepted: 9 January 2007 / Published online: 16 February 2007

Abstract Excited electronic states of the anion radical of *para*-benzoquinone were studied by time dependent density functional theory (TD-DFT) including bulk solvent effects by the polarizable continuum model (PCM). The computed vertical excitation energies for the first four low-lying doublet states are in good agreement with previous post-Hartree–Fock computations. Geometry optimization of excited states and inclusion of solvent effects lead to a remarkable agreement between computed adiabatic transition energies and experimental band maxima. Together with their specific interest, the results point out the reliability of TD-DFT/PCM approach for valence excitations and the need to take geometry relaxation and solvent effects into the proper account for a meaningful comparison between computed and experimental absorption spectra.

Keywords TD-DFT · PCM · solvent effects · UV-vis spectra · *para*-benzoquinone

Contribution to the Fernando Bernardi Memorial Issue.

V. Barone (✉) · R. Improta · G. Morelli
Dipartimento di Chimica and INSTM, Universita' di Napoli "Federico II", Complesso Universitario di Monte S. Angelo, Via Cintia, 80126 Napoli, Italy
e-mail: baronev@unina.it

R. Improta
Istituto di Biostrutture e Bioimmagini - CNR, via Mezzocannone 16, 80134 Napoli, Italy

F. Santoro
Istituto per i Processi Chimico-Fisici – CNR, Area della Ricerca del CNR, via Moruzzi 1, 56124 Pisa, Italy

1 Introduction

Quinones, together with their singly and doubly reduced forms (semiquinone and quinol, respectively) are molecules of considerable biological significance due to their ubiquitary presence as electron transfer (ET) agents, particularly in respiration and photosynthesis [1].

p-Benzoquinone (*p*-BQ) has become the key reference molecule in studying the electronic structures and functions of quinone species. The anionic electronic excited states of this chromophore form a dense ladder of states which play an important role as intermediate steps in ET processes and enhance electron acceptor dynamics in natural systems [2]. The spectra of the anion radical (p-BQ^-) have been recorded in different solvents [3,4], but their features have not yet been fully resolved. This has stimulated a number of quantum mechanical studies of the low-lying excited states of p-BQ^- by the most refined post-Hartree–Fock methods (e.g. CASPT2 [5] or SAC-CI [6]). Although the results delivered by those demanding approaches for the isolated anion radical were quite encouraging, extension of the study to condensed phases and/or to larger systems requires the validation of cheaper approaches. The past few years have seen the increasingly successful application of methods rooted into the density functional theory (DFT) [7] and its time-dependent extension (TD-DFT) [8] to the study of the structure and physico-chemical properties for large molecular systems. The field of application of these approaches is further broadened by their integration with effective mean field treatments of bulk solvent effects (e.g. the polarizable continuum model, PCM [9]) and with classical treatments of specific electrostatic and van der Waals interactions (e.g. the ONIOM approach [10]). Thus, together

with the ongoing improvement of density functionals, it is important to test the most recent implementations (e.g. analytical gradients or state-specific formulations for the PCM/TD-DFT model [11,12]) for the possible application to biological systems in solution. The excited states of organic free radicals are particularly important since, despite some successful application [13], little is known about the reliability of the PCM/TD-DFT approach in this connection. In the following we will show, for the specific case of *p*-BQ^-, that vertical excitation energies in the gas phase are close to their CASPT2 counterparts, and that proper evaluation of geometry relaxation and solvent reaction field leads to results in remarkable agreement with experiments both for absorption and fluorescence spectra in condensed phase.

2 Methods

All computations were carried out with a development version of the Gaussian package [14], using the PBE0 hybrid density functional [15], several basis sets of the Pople series [16], and the unrestricted Kohn–Sham (UKS) approach for open-shell systems. Bulk solvent effects were taken into account by the polarizable continuum model (PCM) [9,17], in which the solvent is represented by a polarizable dielectric medium characterized by the relative dielectric constant of the bulk, and a set of optimized radii (in the present instance, the UAHF radii [18]) are used to build an effective cavity occupied by the solute in the solvent. Geometry optimisations were performed at the PBE0/6-31G(d) level in the gas-phase, and at the PCM/PBE0/6-31G(d) level in solution employing for excited electronic states the recent implementation of TD-DFT and PCM/TD-DFT analytical gradients [11]. Using the above geometries vertical and adiabatic transition energies were computed by different basis sets exploiting in solution the linear response non-equilibrium PCM/TD-DFT approach [19].

3 Results

As a preliminary step, we have checked the reliability of PBE0 calculations in describing the ground state of *p*-BQ^- and of its parent neutral compound *p*-BQ. The main geometric parameters optimized at the PBE0/6-31G(d) level for the ground electronic state of *p*-BQ (see Fig. 1) are close to those issuing from electron diffraction experiments [20] (C1–O, C1–C2, and C2–C3 bond lengths of 1.228 vs. 1.225 Å, 1.481 vs. 1.481 Å, and 1.340 vs. 1.344 Å from computations and experiment, respectively). The PBE0 calculations provide also an accurate estimate of the geometry shifts associated to the addition of an electron to *p*-BQ. The C1–O1 and C2–C3 bond lengths are predicted to increase by ∼0.04 and ∼0.03 Å, whereas C1–C2 bonds shorten by ∼0.035 Å. Those values are very similar to those obtained at the CASSCF level [5] and fully consistent with the indications of Raman Resonance experiments [3], which predict that the frequencies associated to the C2–C3 bond stretching increase upon reduction, while the opposite occurs for those associated to the C1–O1 and C2–C3 stretching modes. Those results can be easily rationalized on the ground of the bonding/antibonding character of the *p*-BQ^- orbital formally containing the unpaired electron ($6\pi\uparrow$ in Fig. 2, see below for the notation). Finally, PBE0 calculations provide a good description of the electron density of *p*-BQ^-. Indeed, the hyperfine and *g* tensors, which critically depend on the electron spin

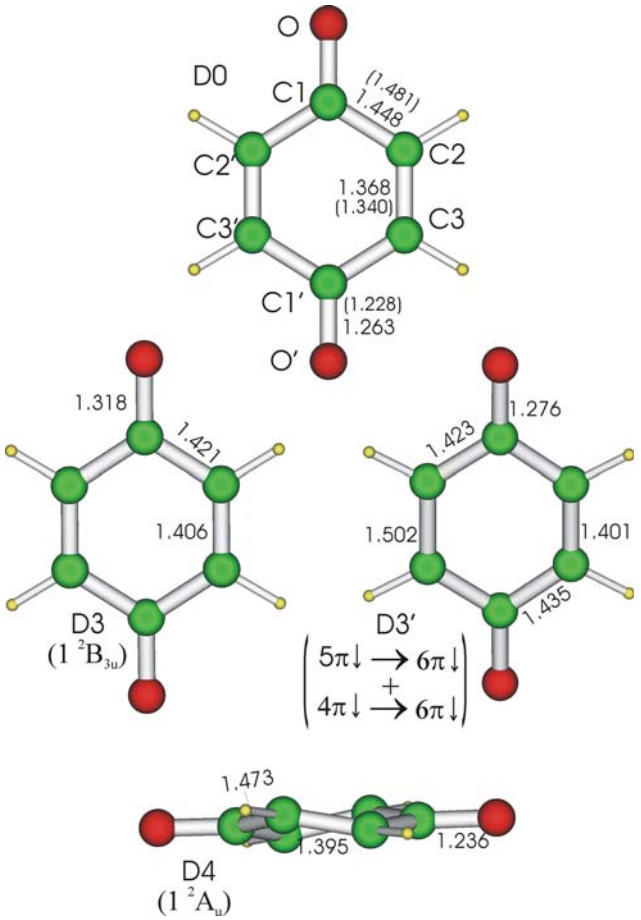

Fig. 1 Optimized structures of the ground and low-energy bright excited states of *p*-BQ^- issuing from PBE0/6-31G(d) and TD-PBE0/6-31G(d) geometry optimizations (see main text for notation and details). Atom labelling and key geometric parameters are also shown. The *values in parentheses* refer to the ground electronic state of the *p*-BQ parent molecule

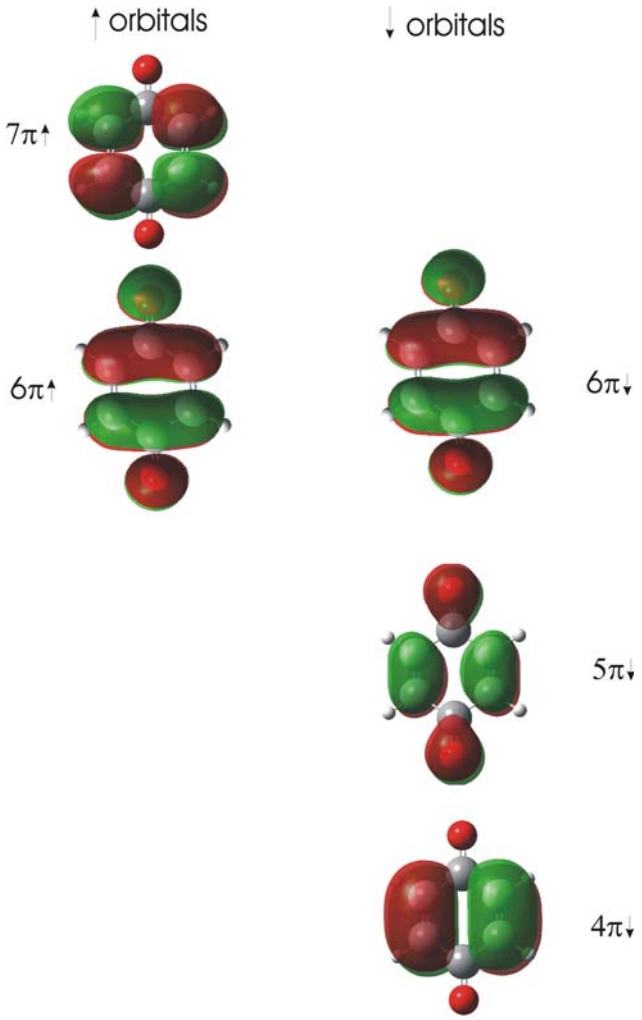

Fig. 2 Schematic drawing of the π and π^* orbitals involved in low-energy bright transitions of p-BQ^- in D_{2h} and C_{2v} point groups

density at the nuclei, computed at the PBE0 level are in excellent agreement with their experimental counterparts [21].

Let us consider that the unpaired electron in the ground electronic state of p-BQ^- has formally spin up (hereafter referred to as ↑) and remember that, in an unrestricted formalism, ↑ and ↓ spin-orbitals are different. In this context, the SOMO is the $6\pi\uparrow$ spin-orbital and the other frontier spin-orbitals dominating the five low-lying excitations found at all computational levels are the empty $7\pi\uparrow$ and $6\pi\downarrow$ spin-orbitals and the occupied $3n\downarrow$, $4n\downarrow$, $4\pi\downarrow$, $5\pi\downarrow$ spin-orbitals. Furthermore, for vertical transitions we can use the symmetry labelling appropriate for the D_{2h} point group of the ground state $1\,^2B_{2g}$ (D0) energy minimum. The first two excited states, D1 ($1\,^2B_{2u}$) and D2 ($1\,^2B_{3g}$), dominated by $4n\downarrow \rightarrow 6\pi\downarrow$ and $3n\downarrow \rightarrow 6\pi\downarrow$ transitions, respectively, are both of n/π^* character and thus, in principle, forbidden. The next couple of states [D3($1\,^2B_{3u}$) and D4 ($1\,^2A_u$)] derives from $5\pi\downarrow \rightarrow 6\pi\downarrow$ and $6\pi\uparrow \rightarrow 7\pi\uparrow$ bright $\pi \rightarrow \pi^*$ transitions. The next state is D5 ($1\,^2B_{1g}$), corresponding to a dark $\pi \rightarrow \pi^*$ ($4\pi\downarrow \rightarrow 6\pi\downarrow$) transition and, finally, a bright D6 ($2\,^2B_{3u}$) state is dominated by the $6\pi\ \uparrow \rightarrow 8\pi\uparrow\ \pi \rightarrow \pi^*$ transition. The π and π^* KS spin-orbitals mentioned above are sketched in Fig. 2.

The anionic nature of the studied species suggests that diffuse functions could play a significant role and this is confirmed by the results collected in Table 1. As a matter of fact, 6-31G(d) transition energies are significantly different from the other ones, whereas extension of the basis set above the 6-31 + G(d,p) level has a negligible effect. Thus, we will explicitly refer, in the following, to 6-31 + G(d,p) results.

In the gas-phase, the TD-DFT vertical excitation energies (VEEs) for these transitions and the excited state descriptions are in fair agreement with previous CASPT2 and SAC-CI computations (in the following collectively referred to as post-Hartree–Fock). Our computations indeed predict the presence of two low-lying dark excited states ($1\,^2B_{2u}$ and $1\,^2B_{3g}$) around 2.3 eV, of two bright states of comparable strength ($1\,^2B_{3u}$ and $1\,^2A_u$) around 3 eV and, finally, of a strong absorbing state ($2\,^2B_{3u}$) around 4 eV. From a quantitative point of view, the difference between TD-DFT and post-Hartree–Fock results is smaller than that between CASPT2 and SAC-CI values. The only significant discrepancy between TD-DFT and CASPT2 calculations concerns the VEE of the $6\pi\ \uparrow \rightarrow 8\pi\ \uparrow$ transition, that is, ca. 0.5 eV higher according to the former approach. Actually the experimental band maximum in DMSO solution is intermediate between the CASPT2 and the TD-DFT gas phase value (see Table 2). The accuracy of TD-PBE0 calculations is a remarkable result in view of the significantly reduced computational burden and much better scaling properties of the TD-DFT approach with respect to post-Hartree–Fock methods. Of course, the choice of the hybrid density functional (PBE0) and the absence of charge transfer (CT) or Rydberg transitions contribute to explaining this success, but it remains noteworthy that valence spectra of open-shell systems are reproduced with good accuracy. Full geometry optimization of all the excited states (see Fig. 1) leads to results in fair agreement with those issuing from CASSCF computations and with the available experimental evidences (essentially derived from RR experiments) [5].

Indeed, passage from the ground to the D4 excited electronic state leads to a slight increase of the C1–C2 and C2–C3 bond lengths together with a small decrease of the C1–O1 bond length. There is also a widening of the C2–C1–C2′ (C3–C1–C3′) and C2–C3–H (C2′–C3′–H) valence angles. In close analogy with CASSCF results

Table 1 Vertical excitation energies (in eV) of *p*-BQ^- computed in the gas phase by TD-DFT, CASPT2, and SAC-CI approaches

State[a]	Main transition	6-31G(d)[a]	6-31 + G(d,p)[a,b]	6-311 + G(2d,2p)[a,b]	CASPT2[c]	SAC-CI[d]
D1 ($1\,^2B_{2u}$)	$4n\downarrow \rightarrow 6\pi\downarrow$	2.23 (0.00)	2.30 (0.00)	2.31 (0.00)	2.23 (0.00)	2.44
D2 ($1\,^2B_{3g}$)	$3n\downarrow \rightarrow 6\pi\downarrow$	2.27 (0.00)	2.35 (0.00)	2.36 (0.00)	2.25 (0.00)	2.38
D3 ($1\,^2B_{3u}$)	$5\pi\downarrow \rightarrow 6\pi\downarrow$	3.11 (0.07)	3.09 (0.08)	3.09 (0.07)	2.80 (0.05)	2.71
D4 ($1\,^2A_u$)	$6\pi\uparrow \rightarrow 7\pi\uparrow$	3.26 (0.05)	3.10 (0.05)	3.05 (0.05)	2.82 (0.10)	3.50
D5 ($1\,^2B_{1g}$)	$4\pi\downarrow \rightarrow 6\pi\downarrow$	3.42 (0.00)	3.32 (0.00)	3.32 (0.00)	3.25 (0.00)	3.75
D6 ($2\,^2B_{3u}$)	$6\pi\uparrow \rightarrow 8\pi\uparrow$	5.28 (0.23)	4.18 (0.10)	4.11 (0.11)	3.56 (0.32)	3.74

Oscillator strengths are given in parenthesis
[a] Symmetry labels refer to D_{2h} point group
[b] Single point TD-PBE0 computations at PBE0/6 -31G(d,p) geometry
[c] From Ref. [5] [d] From Ref. [6]

Table 2 Vertical excitation energies (in eV) for the bright states of *p*-BQ^- computed in solution by the PCM/TD-PBE0 approach are compared with available experimental band maxima

State	Main transition	6-31G(d)[a]	6-31+G(d,p)[a]	6-311+G(2d,2p)[a]	Exp. [b]
CCl_4					
D3 ($1\,^2B_{3u}$)	$5\pi\downarrow \rightarrow 6\pi\downarrow$	3.08 (0.10)	3.06 (0.13)	3.06 (0.12)	
D4 ($1\,^2A_u$)	$6\pi\uparrow \rightarrow 7\pi\uparrow$	3.29 (0.07)	3.19 (0.07)	3.13 (0.07)	
D6 ($2\,^2B_{3u}$)	$6\pi\uparrow \rightarrow 8\pi\uparrow$	5.18 (0.29)	4.15 (0.14)	4.08 (0.13)	
DMSO					
D3 ($1\,^2B_{3u}$)	$5\pi\downarrow \rightarrow 6\pi\downarrow$	3.08 (0.10)	3.08 (0.13)	3.08 (0.12)	2.73
D4 ($1\,^2A_u$)	$6\pi\uparrow \rightarrow 7\pi\uparrow$	3.40 (0.07)	3.35 (0.07)	3.28 (0.06)	≈ 3.10[c]
D6 ($2\,^2B_{3u}$)	$6\pi\uparrow \rightarrow 8\pi\uparrow$	5.18 (0.23)	4.16 (0.104	4.09 (0.15)	3.82

Oscillator strengths are given in parenthesis
[a] Single point PCM/TD-PBE0 computations at PCM/PBE0/6-31G(d,p) geometry
[b] From Ref. [2]
[c] Shoulder at ≈400 nm (see Ref. [4])

[5], the geometry changes involved in the D0 → D4 ($1\,^2A_u$) electron transition can thus be described essentially as a ring breathing.

A remarkable finding issuing from TD-DFT geometry optimizations is that the D4 state is not planar and also this result is indirectly confirmed by CASSCF geometry optimizations, which have been performed within D_{2h} symmetry and indeed exhibit one imaginary frequency for an out- of- plane vibrational mode [5]. This is thus the first time that the true energy minimum for this excited state is located. Small distortion from the ring planarity can help to reduce the geometry strain due to the opening of the C2–C1–C2′ and C3–C1–C3′ valence angles.

When performed within D_{2h} symmetry TD-DFT and CASSCF geometry optimizations provide similar results also for the D3 ($1\,^2B_{3u}$) excited state, which is indeed characterized by a significant increase of the C1-O1 and C2–C3 bond lengths with respect to the ground electronic state, in line with the strong antibonding character of the $6\pi\downarrow$ spin-orbital with respect to those bonds. Since the C1–C2 bond lengths decrease, the quinoid ring is characterized by a benzene-like structure, with six identical carbon–carbon bond lengths of ∼1.4 Å. However, also in this case, unconstrained geometry optimizations provide a somewhat different description. Indeed, when the D_{2h} symmetry is lifted, D3 ($5\pi\downarrow \rightarrow 6\pi\downarrow$) and D5 ($4\pi\downarrow \rightarrow 6\pi\downarrow$) states can interact with a strength increasing with the size of the basis set and the polarity of the embedding medium (vide infra). So, when using the 6-31 + G(d,p) basis set, geometry optimization of the D3 ($5\pi\downarrow \rightarrow 6\pi\downarrow$) state converges to a 'new' excited state (D3′ in Fig. 1), characterized by a C_{2v} energy minimum and receiving significant contributions from both $5\pi\downarrow \rightarrow 6\pi\downarrow$ and $4\pi\downarrow \rightarrow 6\pi\downarrow$ transitions (see Fig. 3). The resulting D3′ energy minimum is planar, but is characterized by a C2–C3 bond much shorter than the C2′–C3′ one, whose length is, in turn, typical of a single carbon–carbon bond.

Let us now come to computations performed in solution: in order to analyse general trends, we have considered two solvents of significantly different polarity, namely CCl_4 and DMSO (only for the latter solvent experimental data are available). Full geometry optimizations lead to structures very similar to those obtained in the gas phase and shown in Fig. 1. However, the results collected in Tables 2 and 3 show that solvent shifts on transition energies are not negligible and that their inclusion leads to results in remarkable agreement with the experiment. In particular, there is a general small blue-shift when the solvent polarity increases, and this

Table 3 0–0 absorption and vertical emission energies (in eV) for the two low-lying bright states of *p*-BQ^- computed in solution at the PCM/TD-DFT level are compared with available band maxima. Oscillator strengths are given in parenthesis

State	Main transitions	6-31G(d)[a]	6-31 + G(d,p)[a]	6-311 + G(2d,2p) [a]	Exp.
Gas phase absorption					
D'_3	$5\pi\downarrow\rightarrow6\pi\downarrow + 4\pi\downarrow\rightarrow6\pi\downarrow$	2.91 (0.11)	2.84 (0.13)	2.88 (0.13)	
D_4	$6\pi\uparrow\rightarrow7\pi\uparrow$	3.01 (0.04)	2.82 (0.04)	2.79 (0.04)	
CCl4 absorption					
D'_3	$5\pi\downarrow\rightarrow6\pi\downarrow + 4\pi\downarrow\rightarrow6\pi\downarrow$	2.85 (0.15)	2.76 (0.20)	2.80 (0.20)	
D_4	$6\pi\uparrow\rightarrow7\pi\uparrow$	3.05 (0.06)	2.90 (0.05)	2.87 (0.05)	
DMSO absorption					
D'_3	$5\pi\downarrow\rightarrow6\pi\downarrow + 4\pi\downarrow\rightarrow6\pi\downarrow$	2.78 (0.04)	2.64 (0.03)	2.67 (0.03)	2.73[b]
D_4	$6\pi\uparrow\rightarrow 7\pi\uparrow$	3.15 (0.07)	3.06 (0.05)	3.02 (0.05)	$\approx$ 3.10[c]
Gas phase emission					
D'_3	$5\pi\downarrow\rightarrow6\pi\downarrow + 4\pi\downarrow\rightarrow6\pi\downarrow$	2.70 (0.11)	2.67 (0.13)	2.67 (0.13)	
D_4	$6\pi\uparrow\rightarrow7\pi\uparrow$	2.51 (0.04)	2.31 (0.04)	2.28 (0.04)	
CCl4 emission					
D'_3	$5\pi\downarrow\rightarrow6\pi\downarrow + 4\pi\downarrow\rightarrow6\pi\downarrow$	2.60 (0.15)	2.56 (0.20)	2.57 (0.20)	
D_4	$6\pi\uparrow\rightarrow7\pi\uparrow$	2.55 (0.06)	2.40 (0.05)	2.36 (0.05)	
DMSO emission					
D'_3	$5\pi\downarrow\rightarrow6\pi\downarrow + 4\pi\downarrow\rightarrow6\pi\downarrow$	2.31 (0.04)	2.18 (0.03)	2.18 (0.03)	
D_4	$6\pi\uparrow\rightarrow7\pi\uparrow$	2.63 (0.06)	2.53 (0.05)	2.48 (0.05)	

[a] TD-PBE0 at PCM/PBE0/6-31G(d,p) geometry
[b] From Ref. [2]
[c] Shoulder at ≈400 nm (see Ref. [4])

feature seems confirmed by experiments (see notes of Table 2 in Ref. [5]). Furthermore, the $4\pi\downarrow\rightarrow 6\pi\downarrow$ transition energy decreases with the polarity of the solvent, and this has a non-negligible effect on the position of the corresponding band in the UV spectrum. This result can be rationalized on the ground of the total electric dipole moment of the different excited states. Although the total electric dipole moment of D3 ($1\,^2B_{3u}$) is vanishing by symmetry, that of D3′ is ∼1.5 D; thus explaining the relative stabilization of this state in DMSO.

Finally, we also report in Table 3 the computed vertical emission energies, which could be compared to experimental fluorescence band maxima. While, unfortunately, these data are not available, it is remarkable that the computed Stokes shifts are quite large.

4 Discussion and concluding remarks

In this paper we have presented the essential results of an integrated TD-DFT/PCM approach for the evaluation of absorption and fluorescence spectra of a prototypical radical anion in solution, i.e. *p*-BQ^-. In agreement with previous CASPT2 results [5], our calculations predict that the two peaks detected in photodetachment spectrum [2] at ∼2.25 and ∼2.4 eV are due to the n/π^* dark electronic transitions to D1 ($1\,^2B_{2u}$) and D2 ($1\,^2B_{3g}$) excited states. On the other hand, our results do not yet allow for an unambiguous assignment of the feature at ∼2.8 eV in the absorption spectra. From the one hand the D0 → $1\,^2B_{3u}$ electronic transition exhibits a larger oscillator strength than the D0 → 1^2A_u electronic transition. Furthermore, an analysis performed at the CASSCF level [5] suggests that the vibrational structure of the former transition is in better agreement with RR experiments. On the other hand, full geometry optimizations shows that lifting of D_{2h} symmetry allows for a strong vibronic interaction between the 1^2B_{3u} and a nearly isoenergetic $1\,^2B_{1g}$ dark state. Furthermore, the reliability of the vibrational analysis performed by the authors in [5] is biased by the D_{2h} symmetry constraint, imposing a planar geometry to the $1\,^2A_u$ state and making impossible the $1^2B_{3u}/1^2B_{1g}$ vibronic interaction. In our opinion, only a vibrational analysis performed taking into account the vibronic interactions among the three excited states lying near 3 eV can allow an unbiased interpretation of the absorption spectra in that region. Finally, PCM/TD-DFT and CASPT2 calculations agree in assigning the strong peak around 4 eV to the D0 → 1^2B_{3u} (π/π^*) transition.

From a methodological point of view, it is important to highlight that TD-DFT vertical excitation energies are in fair agreement with post-HF results, and the same applies to excited state equilibrium geometries, which are, furthermore, fully consistent with the available experimental results. The reasonable computational cost of TD-DFT gradients allows to perform complete excited state geometry optimizations, relaxing all the symmetry constraints. As shown by our results on *p*-BQ^-, this is a very important possibility when dealing

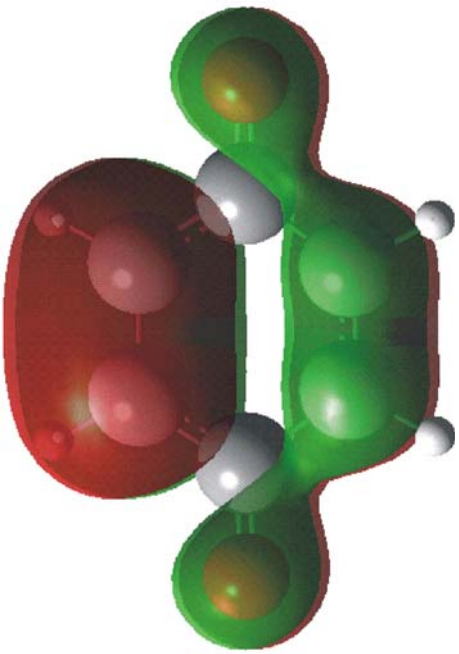

Fig. 3 Schematic drawing of the low-energy occupied π orbital resulting from the combination of $4\pi\downarrow$ and $5\pi\downarrow$ orbitals, when the D_{2h} symmetry is reduced to C_{2v}(D'_3 energy minimum in Fig. 1)

with multiple close-lying excited states, whose relative energy can be extremely sensitive to any enforced symmetry. Finally, inclusion of bulk solvent effects by a non-equilibrium continuum method leads to results in remarkable agreement with their experimental counterparts.

From a more general point of view, our results confirm the reliability of the TD-DFT/PCM approach for valence excitation of large molecular systems including open-shell species. It is well known that current density functionals have limitations for charge transfer and Rydberg excitations [22]; however, most experimental studies deal with valence excitations, which are well reproduced by the PBE0 hybrid functional also for open-shell systems. Furthermore, ongoing research in connection with optimized effective potentials (OEP) [23] and asymptotically corrections [24] is paving the route toward effective solutions to these problems. The availability of analytical gradients for TD-DFT allows to take into account geometry relaxation and, when needed, vibronic contributions to electronic spectra [25]. The effective inclusion of solvent effects by continuum or integrated discrete/continuum models in all the above approaches extends the range of application to condensed phases [26,27]. All these features can be coupled to explicit dynamical treatments (both in classical and extended Lagrangian versions) when static or effectively averaged treatments are no longer sufficient and short-time solute–solvent fluctuations need to be explicitly accounted for [28]. While further developments are needed for improving quantitative aspects and for including long-time dynamical effects [29], the integrated approach sketched earlier already represents, in our opinion, a versatile and robust tool for studying the spectroscopic signatures of large systems of biological relevance in their natural environment.

Acknowledgments All the calculations have been performed using the advanced computing facilities of the "Campus Grid" - University Federico II, Naples.

References

1. Patai S (1974) Chemistry of Quinoid compounds. Interscience, New York
2. Schiedt J, Weinkauf R (1999) J Chem Phys 110:304
3. Zhao X, Imahori H, Zhan C-G, Sakata Y, Iwata S, Kitagawa T (1997) J Phys Chem A 101:622
4. Zhao X, Kitagawa T (1998) J Raman Spectrosc 29:773
5. Pou-Amèrigo R, Serrano-Andres L, Merchán M, Ortí E, Forsberg N (2000) J Am Chem Soc 122:6067
6. Honda Y, Hada M, Ehara M, Nakatsuji H (2002) J Phys Chem A 106:3838
7. Koch W, Holthausen MC (2001) A chemist's guide to density functional theory, 2nd ed. Wiley-VCH, Weinheim
8. Marques MAL, Gross EKU (2004) Annu Rev Phys Chem 55:427
9. Tomasi J, Mennucci B, Cammi R (2005) Chem Rev 105:2999
10. Dapprich S, Komaromi I, Byun KS, Morokuma K, Frisch MJ (1999) Theochem 461:1
11. Scalmani G, Frisch MJ, Mennucci B, Tomasi J, Cammi R, Barone V (2006) J Chem Phys 124:094107
12. Improta R, Barone V, Scalmani G, Frisch MJ (2006) J Chem Phys 125:054103
13. Adamo C, Barone V (1999) Chem Phys Lett 314:152
14. Frisch MJ et al. (2003) Gaussian 03, Revision C.02. Gaussian, Inc., Wallingford
15. Adamo C, Barone V (1999) J Chem Phys 110:6158
16. Foresman JB, Frisch AE (1996) Exploring chemistry with electronic structure methods, 2nd edn. Gaussian Inc., Pittsburgh
17. Cossi M, Scalmani G, Rega N, Barone V (2002) J Chem Phys 117:43
18. Barone V, Cossi M, Tomasi J (1997) J Chem Phys 107:3210
19. Cossi M, Barone V (2001) J Chem Phys 115:4708
20. Hagen K, Hedberg K (1973) J Chem Phys 59:158
21. Mattar SM (2004) J Phys Chem B 108:9449
22. Drew A, Weisman JL, Head-Gordon M (2003) J Chem Phys 119:2943
23. Della Sala F, Görling A (2001) J Chem Phys 115:5718
24. Yanai T, Tew DP, Handy N (2004) Chem Phys Lett 393:51
25. Dierksen M, Grimme SS (2005) J Chem Phys 122:244101
26. Gustavsson T, Banyasz A, Lazzarotto E, Markovitsi D, Scalmani G, Frisch MJ, Improta R, Barone V (2006) J Am Chem Soc 128:607
27. Improta R,Barone V, Santoro F (2007) Angew Chem 46:405
28. Pavone M, Cimino P, De Angelis F, Barone V (2006) J Am Chem Soc 128:4338
29. Barone V, Polimeno A (2006) Phys Chem Chem Phys 8:4609